JACS
JOURNAL OF THE AMERICAN CHEMICAL SOCIETY
Article
pubs.acs.org/JACS

Mechanistic Study of Chemoselectivity in Ni-Catalyzed Coupling Reactions between Azoles and Aryl Carboxylates

Qianqian Lu,[†,§] Haizhu Yu,[‡,§] and Yao Fu*[,†]

[†]Department of Chemistry, University of Science and Technology of China, Hefei 230026, PR China
[‡]Department of Polymer Science and Engineering, University of Science and Technology Beijing, Beijing 100083, PR China

Supporting Information

ABSTRACT: Itami et al. recently reported the C−O electrophile-controlled chemoselectivity of Ni-catalyzed coupling reactions between azoles and esters: the decarbonylative C−H coupling product was generated with the aryl ester substrates, while C−H/C−O coupling product was generated with the phenol derivative substrates (such as phenyl pivalate). With the aid of DFT calculations (M06L/6-311+G(2d,p)-SDD//B3LYP/6-31G(d)-LANL2DZ), the present study systematically investigated the mechanism of the aforementioned chemoselective reactions. The decarbonylative C−H coupling mechanism involves oxidative addition of C(acyl)−O bond, base-promoted C−H activation of azole, CO migration, and reductive elimination steps (C−H/Decar mechanism). This mechanism is partially different from Itami's previous proposal (Decar/C−H mechanism) because the C−H activation step is unlikely to occur after the CO migration step. Meanwhile, C−H/C−O coupling reaction proceeds through oxidative addition of C(phenyl)−O bond, base-promoted C−H activation, and reductive elimination steps. It was found that the C−O electrophile significantly influences the overall energy demand of the decarbonylative C−H coupling mechanism, because the rate-determining step (i.e., CO migration) is sensitive to the steric effect of the acyl substituent. In contrast, in the C−H/C−O coupling mechanism, the release of the carboxylates occurs before the rate-determining step (i.e., base-promoted C−H activation), and thus the overall energy demand is almost independent of the acyl substituent. Accordingly, the decarbonylative C−H coupling product is favored for less-bulky group substituted C−O electrophiles (such as aryl ester), while C−H/C−O coupling product is predominant for bulky group substituted C−O electrophiles (such as phenyl pivalate).

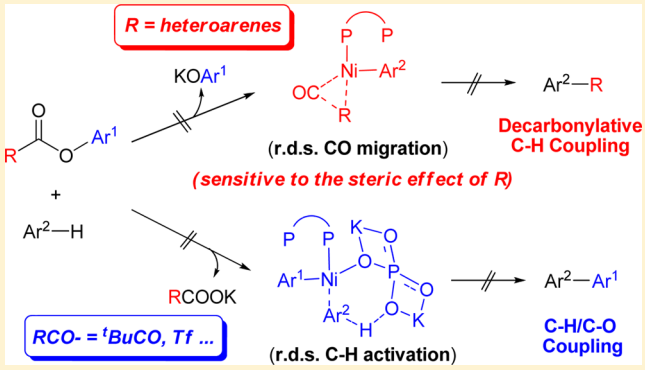

1. INTRODUCTION

Bi(hetero)aryls widely exist in natural substances,[1] pharmaceutical molecules[2] and materials,[3] hence the preparation of bi(hetero)aryls is of great importance. In the past decades, transition-metal-catalyzed cross-coupling reactions between (hetero)aryl halides and (hetero)arylmetallic reagents have been widely used to synthesize bi(hetero)aryls.[4] Nevertheless, the development of more efficient and green catalytic systems remains requisite, due to the shortcomings of the cross-coupling reactions (such as the high cost of organometallic substrates). In 2006, a pioneering study describing a transition-metal-catalyzed decarboxylative coupling between aryl carboxylic acids and aryl halides was reported by Goossen and co-workers.[5] Then much effort has been paid to the low-cost and readily accessible aroyl compounds, from which arylmetallic reagents could be generated through decarboxylation[6] or decarbonylation process.[7] More importantly, with the development of C−H activation/functionalization,[8] transition-metal-catalyzed decarboxylative or decarbonylative coupling reactions between aroyl derivatives and simple (hetero)arenes become an effective method to construct C(heteroaryl)−C(heteroaryl) bonds. For example, Crabtree et al. described the Pd-catalyzed decarboxylative C−H coupling between (hetero)arenes and aryl carboxylic acids.[9] Yu et al. reported the Rh(I)-catalyzed decarbonylative C−H coupling of (hetero)arenes with acid chlorides.[10] Recently Itami et al. developed the $Ni(cod)_2$/dcype catalyzed coupling reactions of aryl esters and azoles, and the decarbonylative C−H coupling products were finally obtained (Scheme 1a).[11] Interestingly, in a similar catalytic system (Scheme 1b), a distinct C−H/C−O coupling reaction occurred when using the phenol derivatives (such as triflates, carbamates, tosylates, and sulfamates) as electrophiles.[12] Itami's reactions provide an efficient way to synthesize bioactive compounds (e.g., muscoride A) and also reveal an interesting chemoselectivity by using different C−O electrophiles.

As to the mechanism of the fascinating chemoselectivity shown in Scheme 1, Itami et al. proposed that the different mechanisms might be responsible for different coupling reactions. The decarbonylative C−H coupling reaction was

Received: December 16, 2013
Published: May 13, 2014

dx.doi.org/10.1021/ja4127455 | J. Am. Chem. Soc. 2014, 136, 8252−8260

Scheme 1. Ni-Catalyzed Coupling Reactions between Azoles and Different Types of Esters

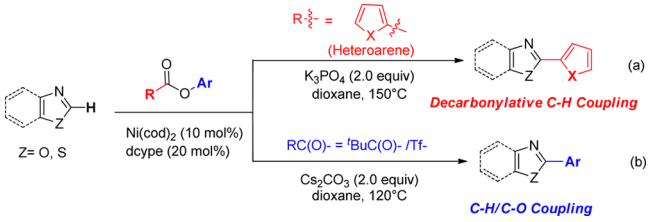

suggested to occur via the oxidative addition of C(acyl)−O bond, CO migration, azole C−H nickelation, reductive elimination, and CO extrusion steps (Decar/C−H mechanism, Figure 1).[11] The C−H/C−O coupling reaction was proposed to begin with the oxidative addition of C(phenyl)−O bond, following with the C−H nickelation and reductive elimination steps (C−H/C−O mechanism, Figure 1).[12] Meanwhile, the azole C−H nickelation step was proposed to be unlikely the rate-determining step of the decarbonylative C−H coupling reaction, because no significant kinetic isotope effect (KIE) was observed (KIE = 1.24).

Despite of the aforementioned mechanistic understandings, many details remain ambiguous. First, the details of decarbonylative C−H coupling mechanism (including the sequence of CO migration, C−H activation process, and the effects of base) are unclear. Second, the oxidative addition of different C−O bonds (C(acyl)−O or C(phenyl)−O bond) causes different mechanisms, whereas the driving force for oxidative addition of the stronger C(phenyl)−O bond (relative to C(acyl)−O bond)[13] in the C−H/C−O coupling reaction remains unknown. More importantly, the reasons for the C−O electrophile-mediated chemoselectivity need to be clarified.

To settle the above problems, we conducted a mechanistic study on Ni-catalyzed coupling reaction between azoles and aryl carboxylates (Scheme 1) using DFT method. The calculation results indicate that Itami's previous proposal (Decar/C−H mechanism in Figure 1) is unfavorable, because the Ni(II) center generated from the CO migration step is electron deficient and disfavors the subsequent C−H activation process. Alternatively, a prior C−H activation (of azole) before the CO migration step can avoid this problem. As a result, the most feasible mechanism for decarbonylative C−H coupling reaction involves the oxidative addition of C(acyl)−O bond, C−H activation of azole, CO migration, and reductive elimination steps (C−H/Decar mechanism). On the other hand, the C−H/C−O coupling reaction proceeds through the oxidative addition of C(phenyl)−O bond, C−H activation of azole (i.e., the rate-determining step), and reductive elimination steps (in accord with the Itami's previous proposal[14] in Figure 1). The steric hindrance of the C−O electrophile significantly suppresses the CO migration step in the C−H/Decar mechanism, and results in the relative priority of the C−H/C−O coupling reaction. In other words, decarbonylative C−H coupling product is favored for less-bulky group substituted C−O electrophiles (such as aryl ester), while C−H/C−O coupling product is predominant for bulky group substituted C−O electrophiles (such as phenyl pivalate).

2. COMPUTATIONAL METHODS

All the DFT calculations were performed with Gaussian09 package.[15] The geometry optimizations of all species in this study were performed using B3LYP method.[16] The 6-31G(d) basis set was used for all the atoms except Ni and K, for which the LANL2DZ basis set[17] was applied (BSI). Frequency calculations at the B3LYP/BSI level of theory were carried out to characterize each stationary point (minimum or transition state) and to obtain the thermodynamic corrections to Gibbs free energy. Intrinsic reaction coordinate (IRC)[18] was calculated to confirm the connection between the transition state and the right reactant/product. Solvent effect was considered by employing the single-point calculations on the gas-phase optimized geometries with SMD model[19] and 1,4-dioxane solvent. All the single-point calculations were performed with M06-L/BSII level[20] (BSII designates the combination of 6-311+G(2d,p) for C, H, O, P, S, N and SDD[21] for Ni, K). The additional polarization functions were Ni($\zeta(f)$) = 3.130, and K($\zeta(d)$) = 1.000.[22] The reported Gibbs free energy in this study was calculated by adding the gas-phase Gibbs free energy correction with the solution-phase single-point energy.[23,24]

3. RESULT

In this study, the coupling reactions between benzoxazole (**azole**) and phenyl thiophene-2-carboxylate (**ester-1**) or phenyl pivalate (**ester-2**) catalyzed by Ni(cod)$_2$/dcype were chosen as the model reactions (eqs 1 and 2).

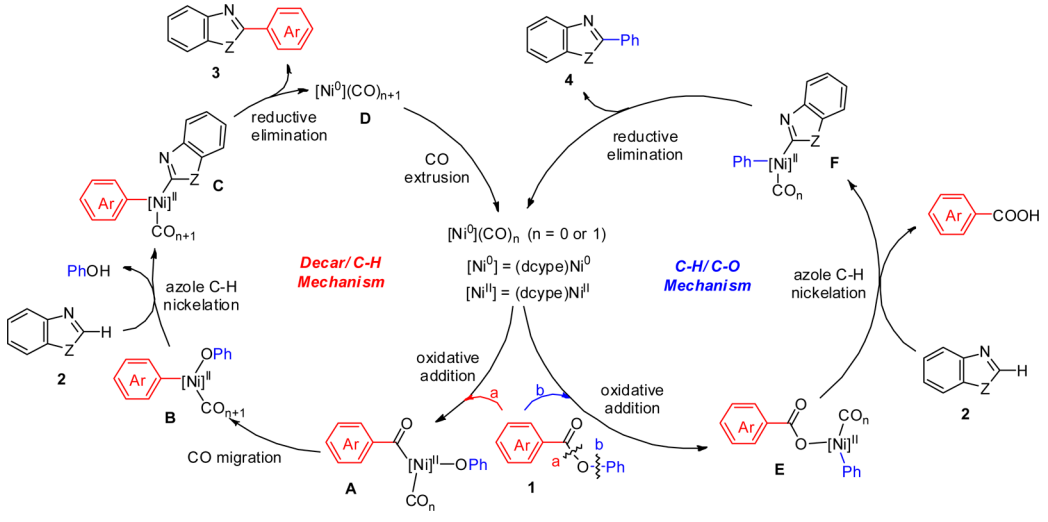

Figure 1. Proposed mechanisms of the Ni-catalyzed coupling reaction between aryl ester (**1**) and azole (**2**).

dx.doi.org/10.1021/ja4127455 | J. Am. Chem. Soc. 2014, 136, 8252−8260

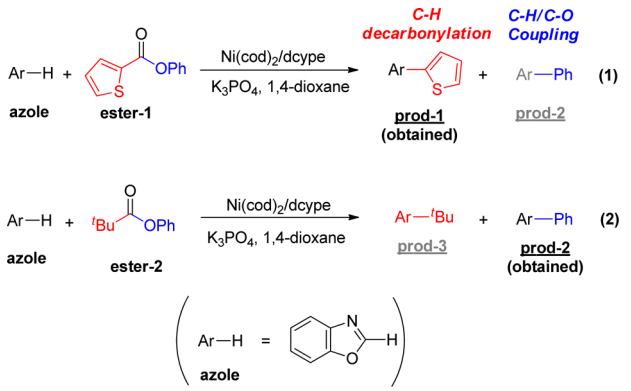

For clarity reasons, the following discussions are divided into two parts: the decarbonylative C−H coupling mechanism and the C−H/C−O coupling mechanism.

3.1. Decarbonylative C−H coupling mechanism. In this section, we took the transformation of eq 1 as an example to discuss the detailed elementary steps. The intermediates/transition states in catalytic cycles of eqs 1 and 2 are named as **P-Int*/P-TS*** and **T-Int*/T-TS***, respectively.

3.1.1. Decar/C−H Mechanism of Eq 1. Oxidative Addition of C(acyl)−O Bond. According to the calculation results, the coordination of the thienyl group of **ester-1** to Ni(dcype) occurs first to form the reactant−catalyst complex **P-Int1** (Figure 2). Then **P-Int1** goes through isomerization[25] to

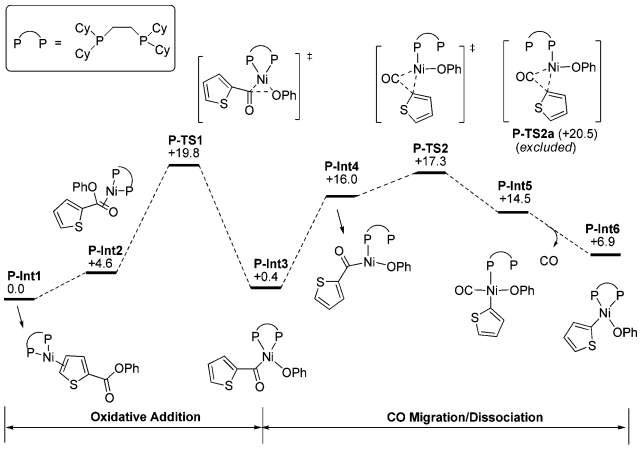

Figure 2. Oxidative addition and CO migration steps involved in Decar/C−H mechanism of eq 1.

produce the η^2-coordinated complex **P-Int2** (ΔG = +4.6 kcal/mol), from which oxidative addition occurs via the three-centered transition state **P-TS1** to give the square-planar intermediate **P-Int3** (ΔG = +0.4 kcal/mol). As shown in Figure 2, the oxidative addition of C(acyl)−O bond is reversible, and its energy barrier is +19.8 kcal/mol.

CO Migration and CO Dissociation. From **P-Int3**, the dissociation of one arm of the bidentate phosphine ligand (dcype) occurs first to provide a vacant site and facilitate the CO migration step.[26] This step gives a T-shaped intermediate **P-Int4**, and the subsequent CO migration occurs via the transition state **P-TS2** (ΔG = +17.3 kcal/mol). From the immediate product of CO migration (**P-Int5**), CO dissociation occurs easily to form the bidentate ligand coordinated intermediate **P-Int6**, and this step is exergonic by 7.6 kcal/mol.[27,28] Note that in the present study, some other possible CO migration processes (such as the involvement of **P-TS2a**, Figure 2) have also been examined. Nonetheless, these possibilities have been excluded due to the high-energy demands (please see SI for more details).

Azole C−H Nickelation. From **P-Int6**, benzoxazole (**azole**) would participate into the catalytic cycle to carry on the C−H nickelation step, and three possible pathways were proposed for this process (Scheme 2).

The first C−H nickelation pathway involves the direct activation of **azole** C−H bond with the intramolecular PhO^- of **P-Int6** (Scheme 2a). In this pathway, the dissociation of one arm of the diphosphine ligand and the coordination of **azole** occur to form **P-Int7**. Subsequently, **P-Int7** undergoes a four-centered C−H activation transition state **P-TS3** to produce the Ni(II) complex **P-Int8**. The high energy barrier of +58.3 kcal/mol precludes the possibility of this pathway.

As the partial dissociation of dcype causes the instability of the Ni(II) complexes, the intermolecular PhO^- assisted azole C−H activation pathway was next studied. As shown in Scheme 2b, the coordinated complex **P-Int7a** is first formed through the weak interaction between O atom (in **P-Int6**) and H atom (in **azole**). Subsequently, the C−H activation transition state **P-TS3a** occurs to generate the deprotonated product **P-Int8a**. Although the energy barrier of **P-TS3a** ($\Delta G^{\ddagger}$ = +47.8 kcal/mol) is ∼10 kcal/mol lower than that of **P-TS3** ($\Delta G^{\ddagger}$ = +58.3 kcal/mol), it is still high for the coupling reaction to occur at 150 °C.[11] Thus, the PhO^- assisted C−H activation pathways (either via intermolecular or intramolecular pathways) were excluded.

Considering that the base promoted C−H activation has been previously proposed,[29] we also examined the possibility of the $K_2PO_4^-$ promoted azole C−H activation in the present study. According to the calculation results (Scheme 2c), the ligand exchange between −OPh and $K_2PO_4^-$ occurs first to generate **P-Int7b**.[30] Thereafter, the partial dissociation of dcype, rearrangement of $K_2PO_4^-$, and the ligation of Ar−H occur subsequently to generate **P-Int8b** (all these steps are quite facile, and the details are given in SI). After that, the C−H bond of **azole** was deprotonated by $K_2PO_4^-$ via the six-centered transition state **P-TS3b** to give **P-Int9**. During the transformation from **P-Int8b** to **P-TS3b**, the Ni−O2 bond distance is lengthened from 1.918 to 2.340 Å (Figure 3), the Ni−C distance is shortened from 3.767 to 2.662 Å, and the forming O2−H bond length is 1.012 Å in **P-TS3b**. All these structural parameters are consistent with the formal concerted metalation/deprotonation mechanism (CMD C−H activation mechanism).[31] What's more important, the relative free energy of **P-TS3b** (ΔG = +29.2 kcal/mol) is lower than that of **P-TS3** and **P-TS3a**, therefore it is more plausible in describing the C−H nickelation of azole.

Reductive Elimination. The product of C−H nickelation (i.e., **P-Int9**) then dissociates K_2HPO_4 to generate the square-planar intermediate **P-Int10** (ΔG = +5.4 kcal/mol, Figure 4). Then reductive elimination occurs via the four-coordinated transition state **P-TS4** to give **P-Int11** (ΔG = −3.3 kcal/mol).[32,33] Finally, the ligand exchange process between **P-Int11** and **ester-1** occurs to release **prod-1** and regenerate the Ni(0) complex **P-Int1**.

The Overall Picture of Decar/C−H Mechanism of Eq 1. For clarity reasons, the key species in Decar/C−H mechanism of eq 1 are given in Figure 4. First, oxidative addition of C(acyl)−O bond of **ester-1** occurs with an energy barrier of +19.8 kcal/mol. Then the formed intermediate **P-Int3** undergoes CO

dx.doi.org/10.1021/ja4127455 | J. Am. Chem. Soc. 2014, 136, 8252−8260

Scheme 2. Three Possible Azole C−H Nickelation Pathways on P-Int6

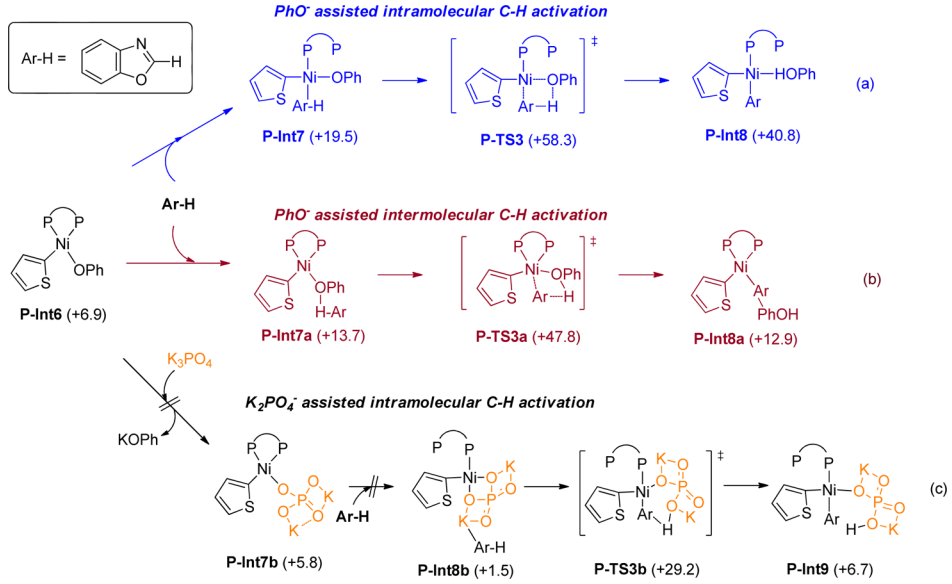

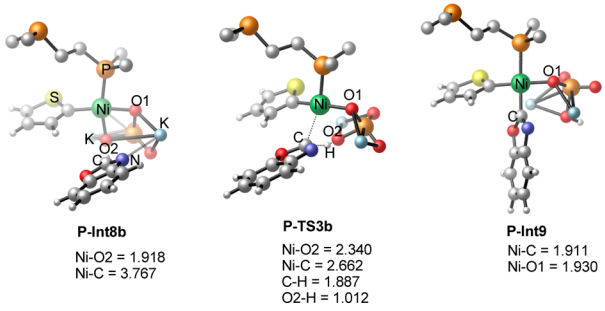

Figure 3. Optimized structures of **P-Int8b**, **P-TS3b**, and **P-Int9**. The bond lengths are given in Å. For clarity, the cyclohexanes of ligand are omitted in this and the following figures.

migration−dissociation step (**P-Int3** → **P-TS2** → **P-Int6**), and this step needs to overcome an energy barrier of +17.3 kcal/mol. Subsequently, azole C−H nickelation (**P-Int6** → **P-TS3b** → **P-Int10**) and reductive elimination steps occur (**P-Int10** → **P-TS4** → **P-Int11**), and their energy barriers are +29.2 and +19.6 kcal/mol, respectively. The C−H nickelation (with an energy barrier of +29.2 kcal/mol) represents the rate-determining step. Interestingly, this conclusion is inconsistent with Itami's previous studies (KIE = 1.24).[11] In this context, we wondered if there are other more plausible decarbonylative C−H coupling mechanisms.

3.1.2. C−H/Decar Mechanism of Eq 1. Different from the Decar/C−H mechanism in Section 3.1.1, the C−H nickelation of azole might possibly occur before the CO migration step, and this pathway is named as C−H/Decar Mechansim.

The oxidative addition step involved in C−H/Decar mechanism is the same as that of Decar/C−H mechanism (Figure 4). Thereafter, the C−H nickelation on the immediate product of oxidative addition step (**P-Int3**) occurs favorably with the aid of $K_2PO_4^-$. As shown in Figure 5, PhO^- of **P-Int3**

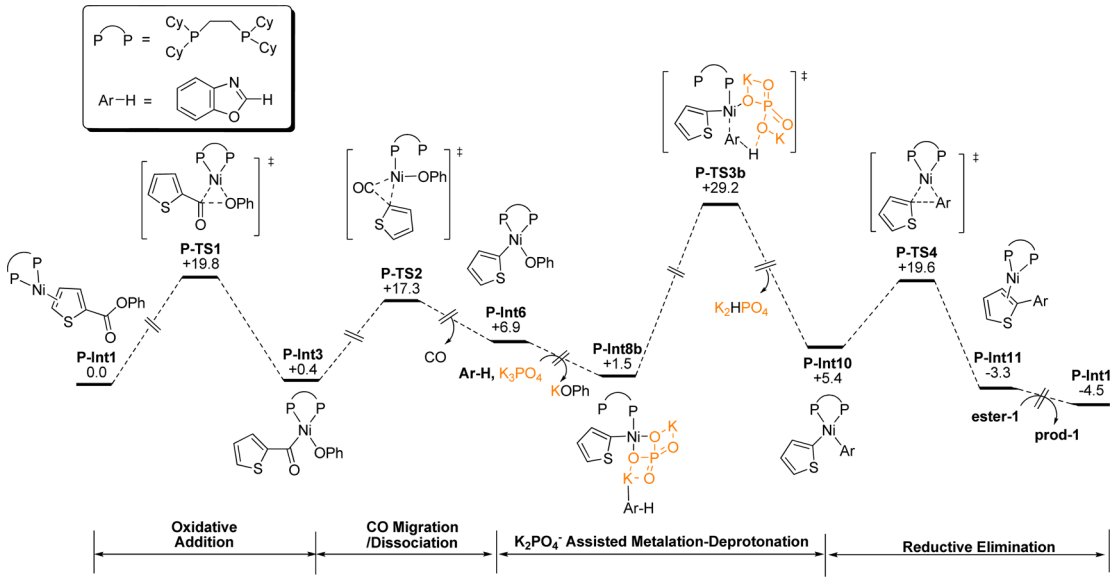

Figure 4. Energy profiles of Decar/C−H mechanism of eq 1.

dx.doi.org/10.1021/ja4127455 | J. Am. Chem. Soc. 2014, 136, 8252−8260

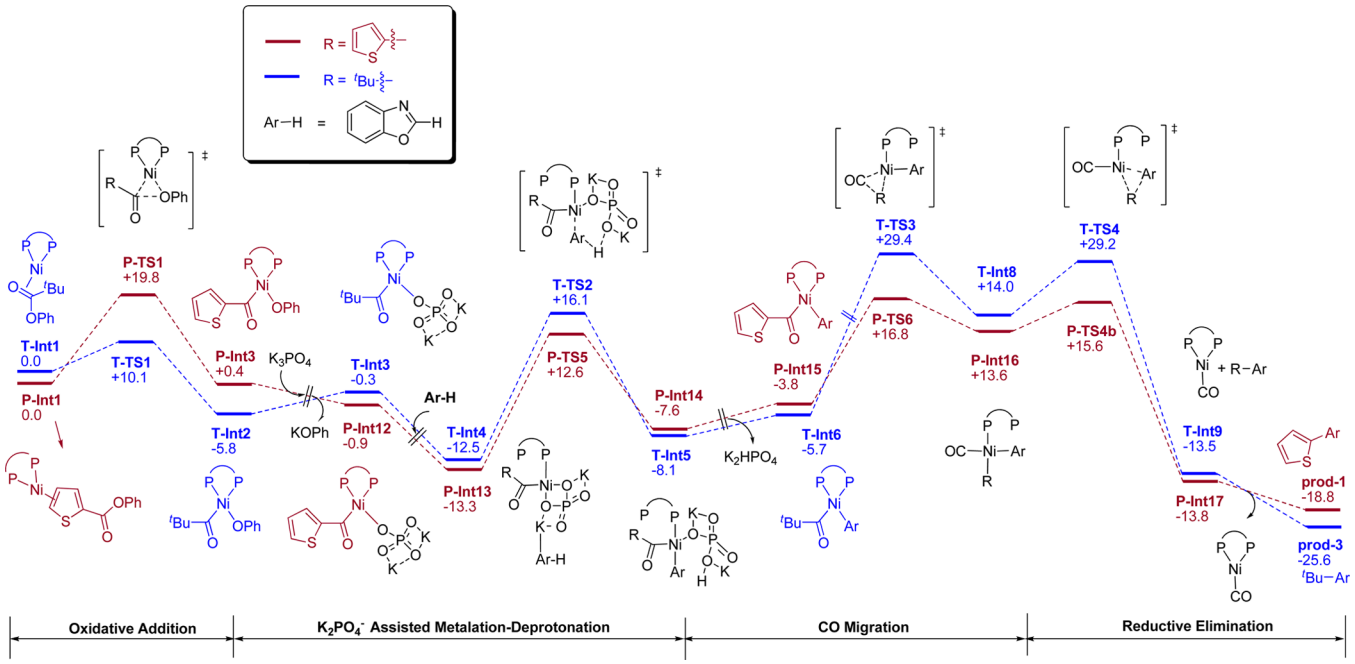

Figure 5. Energy profiles of C–H/Decar mechanism of eqs 1 (red) and 2 (blue).

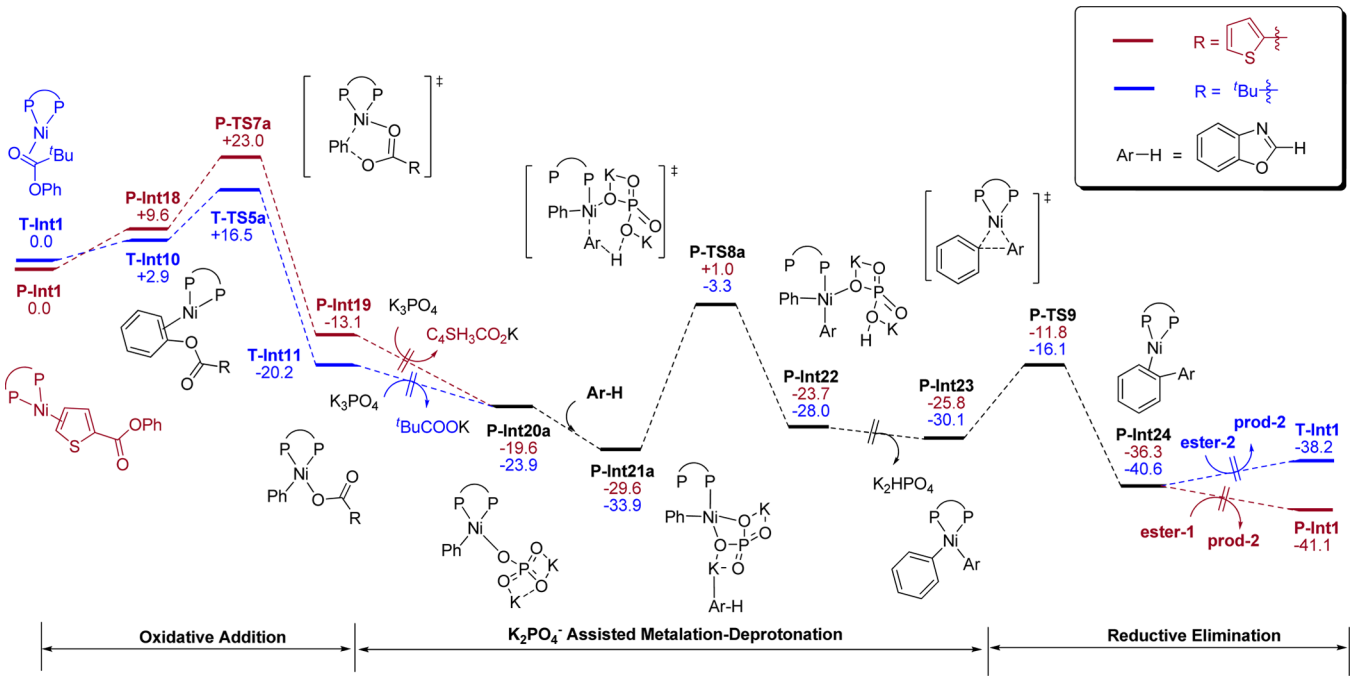

Figure 6. Detailed energy profiles of C–H/C–O mechanism of eqs 1 (red) and 2 (blue).

exchanges with $K_2PO_4^-$ to form **P-Int12**, from which the coordination of **azole** enables the generation of the intermediate **P-Int13** (this step is exergonic by 12.4 kcal/mol). Subsequently, a six-membered concerted metalation/deprotonation transition state **P-TS5** occurs to produce the deprotonated complex **P-Int14**. Then dissociation of K_2HPO_4 from **P-Int14** leads to the generation of the bidentate ligand coordinated complex **P-Int15**. After that, **P-Int15** undergoes the CO migration step via the tetra-coordinated transition state **P-TS6** to generate the nickel carbonyl complex **P-Int16** (ΔG = +13.6 kcal/mol), and the energy barrier of CO migration is +30.1 kcal/mol (**P-Int13** → **P-TS6**). From **P-Int16**, the direct reductive elimination step occurs via the transition state **P-TS4b** ($\Delta G^{\ddagger}$ = +28.9 kcal/mol).[34,35] The formed **P-Int17** then easily dissociates **prod-1** to form (dcype)Ni(CO), from which the coordination of **ester-1** and the CO extrusion easily occur to regenerate the Ni(0) complex **P-Int1** (the details have been given in SI).

3.1.3. Comparison of Decar/C–H Mechanism with C–H/Decar Mechanism of Eq 1. According to Figures 4 and 5, the Decar/C–H and C–H/Decar mechanisms of eq 1 share the same oxidative addition step (**P-Int1** → **P-Int3**), while the subsequent transformations are totally different. Based on the above discussions, **P-Int3** easily transforms into the thermody-

dx.doi.org/10.1021/ja4127455 | J. Am. Chem. Soc. 2014, 136, 8252–8260

namically stable intermediate **P-Int13** (Figure 5), which determines the overall activation barriers of these two decarbonylative C−H coupling mechanisms (energetic span model).[36] In this context, the rate-determining steps of Decar/C−H and C−H/Decar mechanisms are C−H activation and CO migration steps, and their overall activation barriers are +42.5 (**P-Int13** → **P-TS3b**) and +30.1 kcal/mol (**P-Int13** → **P-TS6**), respectively. Therefore, C−H/Decar mechanism is relatively more favorable. In addition, the rate-determining step of CO migration agrees with Itami's experimental observations, including both the insignificant KIE values and the greatly decreased yield of decarbonylative C−H coupling product under CO atmosphere.[11]

3.1.4. C−H/Decar Mechanism of Eq 2. Following the discussions on the decarbonylative C−H coupling mechanism of eq 1, the detailed energy profiles of the C−H/Decar mechanism of eq 2 have also been examined (Figure 5).

As shown in Figure 5, the C−H/Decar mechanism of eq 2 is similar to that of eq 1, consisting of oxidative addition of C(acyl)−O bond (**T-Int1** → **T-TS1** → **T-Int2**), $K_2PO_4^-$ assisted metalation/deprotonation (**T-Int2** → **T-TS2** → **T-Int5**), CO migration (**T-Int5** → **T-TS3** → **T-Int8**), and reductive elimination (**T-Int8** → **T-TS4** → **T-Int9**) steps.[37] The rate-determining step of C−H/Decar mechanism of eq2 is the CO migration step, and its overall activation barrier is +41.9 kcal/mol (**T-Int4** → **T-TS3**).

3.2. C−H/C−O Coupling Mechanism. As mentioned in Introduction section, the C−H/C−O mechanism includes the oxidative addition of C(phenyl)−O bond, azole C−H nickelation, and reductive elimination steps. Note that the C−H/C−O mechanisms of eqs 1 and 2 converge at the precursor of the azole C−H nickelation step, because different carboxylate groups (i.e., thiophene-2-carboxylate in eq 1 and pivalate in eq 2) have been released. For comparison, the detailed energy profiles of both of them are given in Figure 6.

3.2.1. Oxidative Addition of C(phenyl)−O Bond. Before the cleavage of C(phenyl)−O bond of **ester-1**, the relatively stable intermediate **P-Int1** first isomerizes to **P-Int18**, in which the phenyl group of **ester-1** is coordinated to Ni(dcype) in an η^2 manner (Figure 6). From **P-Int18**, two types of oxidative addition transition states are possible. The calculation results indicate that the five-centered transition state is energetically much more favored than the related three-centered one (**P-TS7a** vs **P-TS7**, Figure 7).[38] Similar oxidative addition processes are also applicable to eq 2 (**T-Int1** → **T-TS5a** → **T-Int11**).[39]

3.2.2. Azole C−H Activation. From the product of oxidative addition of C(phenyl)−O bond (**P-Int19** or **T-Int11**),[40] the C−H nickelation can then occur. Similar to the C−H nickelation step of C−H/Decar mechanism, the C−H activation in C−H/C−O mechanism also proceeds favorably with the aid of $K_2PO_4^-$.[41] As shown in Figure 6, the ligand exchange of thiophene-2-carboxylic anion of **P-Int19** with $K_2PO_4^-$ leads to the generation of potassium thiophene-2-carboxylate ($C_4SH_3CO_2K$) and **P-Int20a**, which then coordinates with **azole** to form the precursor of C−H activation (i.e., **P-Int21a**). Subsequently, the six-membered concerted metalation/deprotonation transition state **P-TS8a** occurs to generate the deprotonated product **P-Int22**.

Note that similar $K_2PO_4^-$ promoted C−H nickelation of azole also applies to eq 2, in which the ligand exchange between $K_2PO_4^-$ and *t*BuCOO$^-$ of **T-Int11** produces *t*BuCO$_2$K and **P-Int20a**. Once *t*BuCOOK is released, the subsequent steps involved in C−H/C−O mechanism of eq 2 will be the same as that of eq 1 (as mentioned above). For clarity reasons, all the subsequent species are named as **P-Int*** and **P-TS***, and the relative free energy[42] of all these species in eq 1 are used for the following discussions.

3.2.3. Reductive Elimination. The dissociation of K_2HPO_4 from **P-Int22** produces biaryl Ni(II) complex **P-Int23**, which undergoes the four-coordinated reductive elimination transition state **P-TS9** to generate product-Ni(0) complex **P-Int24** (Figure 6). The energy barrier of reductive elimination is +17.8 kcal/mol (**P-Int21a** → **P-TS9**). Finally, **P-Int24** exchanges with **ester-1** (or **ester-2**) to release C−H/C−O coupling product **prod-2** and regenerate **P-Int1** (or **T-Int1**).

In summary, the C−H/C−O mechanisms of eqs 1 and 2 share the same azole C−H activation and reductive elimination steps, and their difference mainly lies in the oxidative addition of C(phenyl)−O bond. The rate-determining step is the $K_2PO_4^-$ assisted azole C−H activation step (for both eqs 1 and 2), and thus different types of carboxylic esters have little influence on the overall energy barrier of the C−H/C−O mechanism.

4. DISCUSSIONS

4.1. The Chemoselectivity of eqs 1 and 2. To compare the relative facility of the decarbonylative C−H coupling and the C−H/C−O coupling reaction in eqs 1 and 2, the critical intermediates and transition states involved in each reaction system were identified (Figure 8).

As shown in Figure 8a, **P-Int13** is the thermodynamically stable intermediate in the catalytic cycle of eq 1, and the overall energy barriers of C−H/Decar mechanism and C−H/C−O mechanism are +30.1 kcal/mol (**P-Int13** → **P-TS6**) and +36.3 kcal/mol (**P-Int13** → **P-TS7a**), respectively. Therefore, the decarbonylative C−H coupling product (**prod-1**) is the resultant product of eq 1.

According to Figure 8b, **T-Int4** is the thermodynamically stable intermediate, and thus the overall energy barriers of the C−H/Decar and the C−H/C−O mechanisms are +41.9 and +30.6 kcal/mol, respectively. Hence, the C−H/C−O coupling reaction is preferred, and **prod-2** is the predicted coupling product of eq 2.

Both the decarbonylative C−H coupling product in eq 1 and the C−H/C−O coupling product in eq 2 are consistent with the previous experimental results.[11,12]

4.2. Origin of the Observed Chemoselectivity of eqs 1 and 2. On the basis of the consistency between the calculation results and the experimental observations, we next paid efforts to figure out the mechanistic origin of chemoselectivity. Note that in the C−H/C−O mechanism, the release of carboxylates occurs prior to the rate-determining step (i.e., base-promoted C−H activation), and thus the overall energy barrier is less

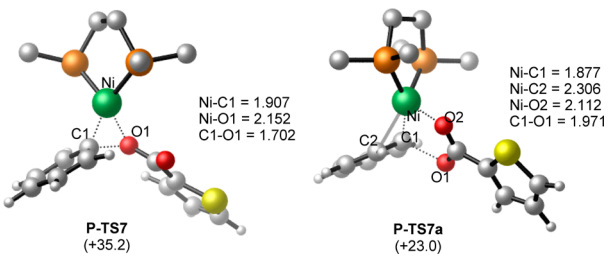

Figure 7. Optimized structures of **P-TS7** and **P-TS7a**.

dx.doi.org/10.1021/ja4127455 | J. Am. Chem. Soc. 2014, 136, 8252−8260

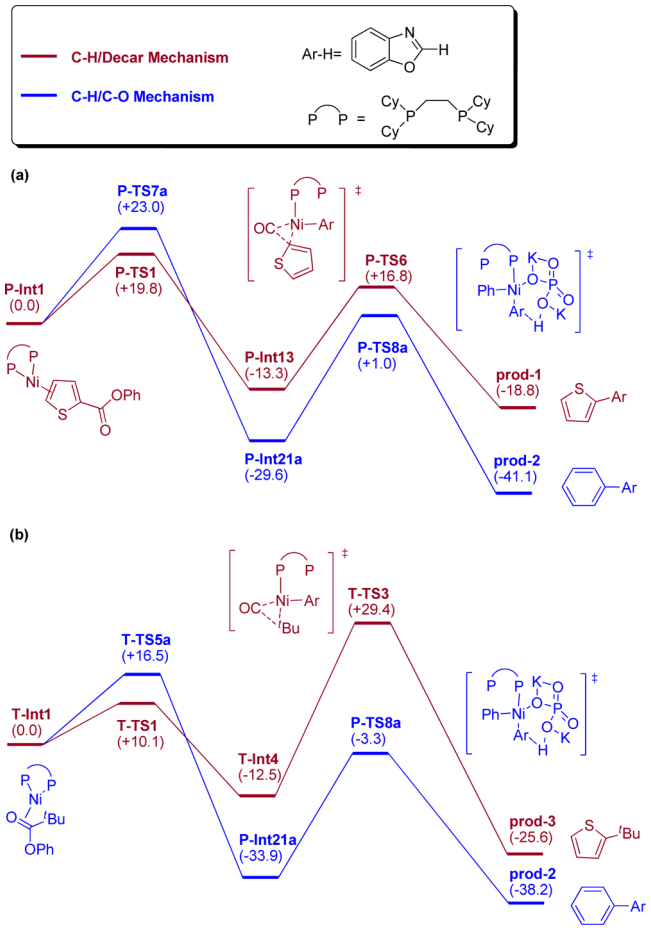

Figure 8. (a) Comparison of C−H/Decar mechanism with C−H/C−O mechanism of eq 1. (b) Comparison of C−H/Decar mechanism with C−H/C−O mechanism of eq 2.

dependent on the acyl substituent. Accordingly, we suggest that the chemoselectivity is mainly caused by the distinct C−H/Decar mechanisms of eqs 1 and 2. Analysis has been performed on the rate-determining step of the C−H/Decar mechanism (CO migration step in Figures 5 and 8).

First, it is noted that the optimized structures of the CO migration transition states **P-TS6** and **T-TS3** (Figure 9) are significantly different. In **P-TS6**, one arm of dcype remains weakly coordinated to the Ni center (Ni−P2 = 2.6076 Å). In contrast, in **T-TS3** the second arm of dcype is totally dissociated from Ni(II) center (Ni−P2 = 5.5894 Å), presumably because of the steric hindrance between the dcype ligand and *t*Bu group. This proposal is supported by the configuration of the heterocyclic ring in these two complexes. In **P-TS6**, the heterocyclic ring (benzoxazolyl) almost parallels to the Ni−P1−C3−C1 plane (N−C3−Ni−P1 = 29.0°), whereas in **T-TS3**, the heterocyclic ring lies almost perpendicular to the Ni−ligand plane to reduce the steric repulsion (N−C3−Ni−P1 = −83.8°).

Second, the steric bulkiness of the *t*Bu group might influence both the steric and electronic effects of CO migration transition state. From steric effect, it results in the significant steric hindrance around the Ni center, withdrawing the coordination of the second arm of the diphosphine ligand and distorting the Ni coordination atmosphere (as mentioned above). From electronic effect, it leads to a more electron-deficient Ni(II) center due to the dissociation of the second arm of dcype and thus disfavors the CO migration process (requires the d → π^* back-bonding interaction from Ni to CO).

To elucidate whether the electronic effect makes an important contribution to the high overall barrier of the *t*Bu-system or not, we carried out the following analysis.

On one hand, the NBO charge analysis on the CO migration transition states with different acyl substituents (Table 1) indicates that the electronic effects of acyl substituents do not show routine relationships with the activation barriers. For example, the NBO charges of the R group vary from −0.057 (in **TS-CH$_3$CO**) to −0.135 (in **TS-p-NO$_2$-C$_6$H$_4$**), while the difference of the concerned activation barriers is only 2 kcal/mol. In addition, Me and *t*Bu groups show similar electronic effects (NBO charge on Me and *t*Bu group is −0.057 and −0.026) and distinct steric effects, while their activation barriers

Table 1. NBO Charges of CO Migration Transition States of R-COOPh

migration group (R group)	$\Delta G^{\ddagger}$ (kcal/mol)	NBO charge on Ni	NBO charge on C	NBO charge on R
thienyl	+20.6	−0.417	−0.391	−0.107
Ph-	+20.5	−0.410	−0.153	−0.096
p-NO$_2$-C$_6$H$_4$-	+20.1	−0.430	−0.132	−0.135
p-Me-C$_6$H$_4$-	+20.7	−0.405	−0.161	−0.086
Me-	+22.6	−0.418	−0.703	−0.057
*t*Bu-	+35.1	+0.051	−0.121	−0.026

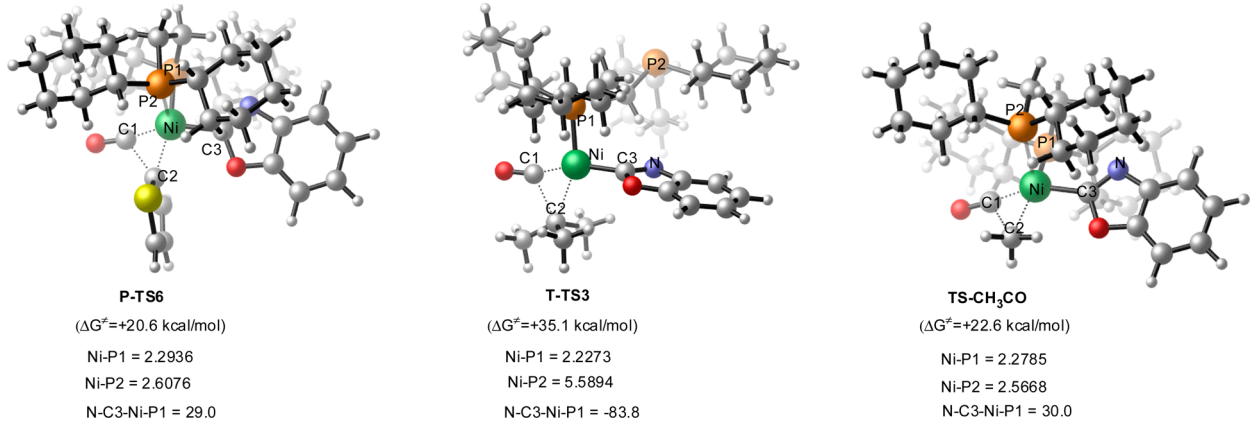

Figure 9. Optimized structures of **P-TS6**, **T-TS3**, and **TS-CH$_3$CO**.

dx.doi.org/10.1021/ja4127455 | J. Am. Chem. Soc. 2014, 136, 8252−8260

are significantly differentiated by 12.5 kcal/mol. On the other hand, the optimized structure (i.e., the configurations of the dcype ligand and the heterocyclic ring in Figure 9) of **TS-CH_3CO** is quite close to those of **P-TS6** (thienyl-system of eq 1), rather than those of **T-TS3** (*t*Bu-system of eq 2). All of these analysis suggest that the steric effect (rather than the electronic effect) significantly disfavors the CO migration step in the *t*Bu-system (eq 2). In this context, the C−H/C−O mechanism becomes more plausible (with an overall activation barrier of about 30 kcal/mol) for *t*Bu system (eq 2), and thus the C−H/C−O coupling product is obtained selectively.

5. CONCLUSIONS

Ni-catalyzed chemoselective decarbonylative C−H coupling (using aryl esters) and C−H/C−O coupling reactions (using phenol derivatives) between azoles and esters are powerful strategies for the preparation of bi(hetero)aryls. To figure out the reasons of this intriguing chemoselectivity, we conducted a DFT study on coupling reactions of benzoxazole and phenyl thiophene-2-carboxylate or phenyl pivalate and gained the following conclusions.

The decarbonylative C−H coupling reaction occurs via oxidative addition of C(acyl)−O bond, base-promoted C−H activation of azole, CO migration (rate-determining step), and reductive elimination steps (C−H/Decar mechanism). This mechanism is relatively more favored than Itami's previous proposal (i.e., Decar/C−H mechanism), because the Ni(II) center generated from the CO migration step is electron-deficient and disfavors the subsequent C−H activation process. Meanwhile, the catalytic cycle of C−H/C−O coupling reaction involves oxidative addition of C(phenyl)−O bond, base-promoted C−H activation of azole (rate-determining step) and reductive elimination steps (similar to Itami's proposal).

The above mechanisms could well explain the experimental observations (including the outcome of the isotope labeling experiments and the effect of CO atmosphere and base). On this basis, the mechanistic origin of the C−O electrophile-controlled chemoselectivity has been analyzed. It was found that the impact of different aryl esters on the decarbonylative C−H coupling mechanism is greater than that on the C−H/C−O coupling mechanism. What's more important, the steric effect (rather than electronic effect) of acyl substituent on different aryl esters significantly affects the energy demands of the decarbonylative C−H coupling reaction. In this context, we concluded that the less-bulky substituted electrophiles favors the decarbonylative C−H coupling reaction, while bulky substituted electrophiles favors the C−H/C−O coupling reaction.

■ ASSOCIATED CONTENT

Supporting Information

Complete ref 15 and computational details. This material is available free of charge via the Internet at http://pubs.acs.org.

■ AUTHOR INFORMATION

Corresponding Author

fuyao@ustc.edu.cn

Author Contributions

[§]These authors contributed equally.

Notes

The authors declare no competing financial interest.

■ ACKNOWLEDGMENTS

We thank the NSFC (21325208, 21172209, 21361140372, 21202006), SRFDP (20123402110051), FRFCU (WK2060190025), CAS (KJCX2-EW-J02), Fok Ying Tung Education Foundation, ChinaGrid project funded by MOE of China, and the super-computer center of Shanghai and USTC.

■ REFERENCES

(1) (a) Nicolaou, K. C.; Bulger, P. G.; Sarlah, D. *Angew. Chem., Int. Ed.* **2005**, *44*, 4442. (b) Hughes, R. A.; Moody, C. J. *Angew. Chem., Int. Ed.* **2007**, *46*, 7930.

(2) (a) Ma, S. K.; Gruber, J.; Davis, C.; Newman, L.; Gray, D.; Wang, A.; Grate, J.; Huisman, G. W.; Sheldon, R. A. *Green Chem.* **2010**, *12*, 81. (b) Chimenti, F.; Maccioni, E.; Secci, D.; Bolasco, A.; Chimenti, P.; Granese, A.; Carradori, S.; Alcaro, S.; Ortuso, F.; Yanez, M.; Orallo, F.; Cirilli, R.; Ferretti, R.; La Torre, F. *J. Med. Chem.* **2008**, *51*, 4874.

(3) (a) Kraft, A.; Grimsdale, A. C.; Holmes, A. B. *Angew. Chem., Int. Ed.* **1998**, *37*, 402. (b) Hoeben, F. J. M.; Jonkheijm, P.; Meijer, E. W.; Schenning, A. P. H. J. *Chem. Rev.* **2005**, *105*, 1491.

(4) (a) Cahiez, G.; Moyeux, A. *Chem. Rev.* **2010**, *110*, 1435. (b) Evano, G.; Blanchard, N.; Toumi, M. *Chem. Rev.* **2008**, *108*, 3054. (c) Littke, A. F.; Fu, G. C. *Angew. Chem., Int. Ed.* **2002**, *41*, 4176. (d) Kotha, S.; Lahiri, K.; Kashinath, D. *Tetrahedron* **2002**, *58*, 9633. (e) Hassan, J.; Sevignon, M.; Gozzi, C.; Schulz, E.; Lemaire, M. *Chem. Rev.* **2002**, *102*, 1359.

(5) (a) Goossen, L. J.; Deng, G. J.; Levy, L. M. *Science* **2006**, *313*, 662. (b) Rodriguez, N.; Goossen, L. J. *Chem. Soc. Rev.* **2011**, *40*, 5030. (c) Shang, R.; Liu, L. *Sci. China Chem.* **2011**, *54*, 1670.

(6) (a) Goossen, L. J.; Rodriguez, N.; Lange, P. P.; Linder, C. *Angew. Chem., Int, Ed.* **2010**, *49*, 1111. (b) Shang, R.; Fu, Y.; Wang, Y.; Xu, Q.; Yu, H. Z.; Liu, L. *Angew. Chem., Int. Ed.* **2009**, *48*, 9350. (c) Shang, R.; Ji, D.-S.; Chu, L.; Fu, Y.; Liu, L. *Angew. Chem., Int. Ed.* **2011**, *50*, 4470. (d) Goossen, L. J.; Zimmermann, B.; Knauber, T. *Angew. Chem., Int. Ed.* **2008**, *47*, 7103. (e) Goossen, L. J.; Rodriguez, N.; Linder, C. *J. Am. Chem. Soc.* **2008**, *130*, 15248. (f) Goossen, L. J.; Rodriguez, N.; Melzer, B.; Linder, C.; Deng, G. J.; Levy, L. M. *J. Am. Chem. Soc.* **2007**, *129*, 4824. (g) Shang, R.; Yang, Z. W.; Wang, Y.; Zhang, S.-L.; Liu, L. *J. Am. Chem. Soc.* **2010**, *132*, 14391. (h) Goossen, L. J.; Linder, C.; Rodriguez, N.; Lange, P. P. *Chem.—Eur. J.* **2009**, *15*, 9336.

(7) (a) Havlik, S. E.; Simmons, J. M.; Winton, V. J.; Johnson, J. B. *J. Org. Chem.* **2011**, *76*, 3588. (b) Yang, L.; Guo, X. Y.; Li, C. J. *Adv. Synth. Catal.* **2010**, *352*, 2899. (c) Goossen, L. J.; Paetzold, J. *Adv. Synth. Catal.* **2004**, *346*, 1665. (d) Stephan, M. S.; Teunissen, A. J. J. M.; Verzijl, G. K. M.; de Vries, J. G. *Angew. Chem., Int. Ed.* **1998**, *37*, 662.

(8) (a) Godula, K.; Sames, D. *Science* **2006**, *312*, 67. (b) Kakiuchi, F.; Chatani, N. *Adv. Synth. Catal.* **2003**, *345*, 1077. (c) Tsang, W. C. P.; Zheng, N.; Buchwald, S. L. *J. Am. Chem. Soc.* **2005**, *127*, 14560. (d) Jordan-Hore, J. A.; Johansson, C. C. C.; Gulias, M.; Beck, E. M.; Gaunt, M. J. *J. Am. Chem. Soc.* **2008**, *130*, 16184. (e) Mei, T. S.; Wang, X.; Yu, J. Q. *J. Am. Chem. Soc.* **2009**, *131*, 10806. (f) Wang, H.; Wang, Y.; Peng, C.; Zhang, J.; Zhu, Q. *J. Am. Chem. Soc.* **2010**, *132*, 13217. (g) Xiao, B.; Gong, T. J.; Liu, Z. J.; Liu, J. H.; Luo, D. F.; Xu, J.; Liu, L. *J. Am. Chem. Soc.* **2011**, *133*, 9250. (h) Wang, X. S.; Leow, D. S.; Yu, J. Q. *J. Am. Chem. Soc.* **2011**, *133*, 13864. (i) Xiao, B.; Gong, T.-J.; Xu, J.; Liu, Z.-J.; Liu, L. *J. Am. Chem. Soc.* **2011**, *133*, 1466. (j) Engle, K. M.; Thuy-Boun, P. S.; Dang, M.; Yu, J. Q. *J. Am. Chem. Soc.* **2011**, *133*, 18183.

(9) Voutchkova, A.; Coplin, A.; Leadbeater, N. E.; Crabtree, R. H. *Chem. Commun.* **2008**, 6312.

(10) Zhao, X. D.; Yu, Z. K. *J. Am. Chem. Soc.* **2008**, *130*, 8136.

(11) Amaike, K.; Muto, K.; Yamaguchi, J.; Itami, K. *J. Am. Chem. Soc.* **2012**, *134*, 13573.

(12) Muto, K.; Yamaguchi, J.; Itami, K. *J. Am. Chem. Soc.* **2012**, *134*, 169.

(13) (a) Quasdorf, K. W.; Tian, X.; Garg, N. K. *J. Am. Chem. Soc.* **2008**, *130*, 14422. (b) Guan, B. T.; Wang, Y.; Li, B. J.; Yu, D. G.; Shi, Z. J. *J. Am. Chem. Soc.* **2008**, *130*, 14468.

(14) Muto, K.; Yamaguchi, J.; Lei, A.; Itami, K. *J. Am. Chem. Soc.* **2013**, *135*, 16384.
(15) Frisch, M. J. et al., *Gaussian 09*, revision B01; Gaussian, Inc.: Wallingford, CT, 2010.
(16) (a) Miehlich, B.; Savin, A.; Stoll, H.; Preuss, H. *Chem. Phys. Lett.* **1989**, *157*, 200. (b) Lee, C. T.; Yang, W. T.; Parr, R. G. *Phys. Rev. B* **1988**, *37*, 785.
(17) Wadt, W. R.; Hay, P. J. *J. Chem. Phys.* **1985**, *82*, 284.
(18) (a) Fukui, K. *Acc. Chem. Res.* **1981**, *14*, 363. (b) Fukui, K. *J. Phys. Chem.* **1970**, *74*, 4161.
(19) Marenich, A. V.; Cramer, C. J.; Truhlar, D. G. *J. Phys. Chem. B* **2009**, *113*, 6378.
(20) Zhao, Y.; Truhlar, D. G. *J. Chem. Phys.* **2006**, *125*, 194101.
(21) Fuentealba, P.; Preuss, H.; Stoll, H.; Vonszentpaly, L. *Chem. Phys. Lett.* **1982**, *89*, 418.
(22) (a) Hollwarth, A.; Bohme, M.; Dapprich, S.; Ehlers, A. W.; Gobbi, A.; Jonas, V.; Kohler, K. F.; Stegmann, R.; Veldkamp, A.; Frenking, G. *Chem. Phys. Lett.* **1993**, *208*, 237. (b) Ehlers, A. W.; Bohme, M.; Dapprich, S.; Gobbi, A.; Hollwarth, A.; Jonas, V.; Kohler, K. F.; Stegmann, R.; Veldkamp, A.; Frenking, G. *Chem. Phys. Lett.* **1993**, *208*, 111.
(23) (a) Liu, L.; Yuan, H.; Fu, T. T.; Wang, T.; Gao, X.; Zeng, Z. P.; Zhu, J.; Zhao, Y. F. *J. Org. Chem.* **2014**, *79*, 80. (b) Lan, Y.; Liu, P.; Newman, S. G.; Lautens, M.; Houk, K. N. *Chem. Sci.* **2012**, *3*, 1987. (c) Zhang, S. L.; Shi, L.; Ding, Y. Q. *J. Am. Chem. Soc.* **2011**, *133*, 20218. (d) Bellarosa, L.; Diez, J.; Gimeno, J.; Lledos, A.; Suarez, F. J.; Ujaque, G.; Vicent, C. *Chem.—Eur. J.* **2012**, *18*, 7749. (e) Yu, H.; Fu, Y. *Chem.—Eur. J.* **2012**, *18*, 16765. (f) Proutiere, F.; Aufiero, M.; Schoenebeck, F. *J. Am. Chem. Soc.* **2012**, *134*, 606. (g) Ford, D. D.; Nielsen, L. P. C.; Zuend, S. J.; Musgrave, C. B.; Jacobsen, E. N. *J. Am. Chem. Soc.* **2013**, *135*, 15595. (h) Nielsen, M. C.; Lyngvi, E.; Schoenebeck, F. *J. Am. Chem. Soc.* **2013**, *135*, 1978. (i) Yi, J.; Lu, X.; Sun, Y.-Y.; Xiao, B.; Liu, L. *Angew. Chem., Int. Ed.* **2013**, *52*, 12409. (j) Suresh, C. H.; Sayyed, F. B. *J. Phys. Chem. A* **2013**, *117*, 10455.
(24) Note that solution-phase optimizations have also been carried out on the key intermediates and transition states, and the results (including energetics and configurations) are in accordance with those of gas-phase optimizations (please see SI for more details).
(25) Please see Figure S1 for more details. For selected study of isomerization among η^2-complexes, see: Yoshikai, N.; Matsuda, H.; Nakamura, E. *J. Am. Chem. Soc.* **2008**, *130*, 15258.
(26) Similar arm-off mechanism of the bidentate phosphine ligands has previously been reported: (a) Clegg, W.; Eastham, G. R.; Elsegood, M. R. J.; Heaton, B. T.; Iggo, J. A.; Tooze, R. P.; Whyman, R.; Zacchini, S. *Organometallics* **2002**, *21*, 1832. (b) Birkholz, M. N.; Freixa, Z.; van Leeuwen, P. W. *Chem. Soc. Rev.* **2009**, *38*, 1099. (c) Hamann, B. C.; Hartwig, J. F. *J. Am. Chem. Soc.* **1998**, *120*, 3694. (d) Kawatsura, M.; Hartwig, J. F. *J. Am. Chem. Soc.* **1999**, *121*, 1473.
(27) All efforts in locating the transition state connecting **P-Int5** and **P-Int6** failed. Nonetheless, this transformation is suggested to be feasible: the energy barrier of CO dissociation from Ni(0) center is calculated to be about +18 kcal/mol, and the thermodynamic stability of higher-valent metal carbonyl complex is relatively lower than that of the low-valent metal carbonyl complex: Crabtree, R. H. *The Organometallic Chemistry of the Transition Metals*, 4th ed.; John Wiley & Sons, Inc.: Hoboken, NJ, 2005. In this context, the energy barrier of CO dissociation from Ni(II) center of **P-Int5** was expected to be even lower.
(28) (a) Yamamoto, T.; Ishizu, J.; Kohara, T.; Komiya, S.; Yamamoto, A. *J. Am. Chem. Soc.* **1980**, *102*, 3758. (b) Li, Z.; Zhang, S.-L.; Fu, Y.; Guo, Q.-X.; Liu, L. *J. Am. Chem. Soc.* **2009**, *131*, 8815.
(29) (a) Larionov, E.; Nakanishi, M.; Katayev, D.; Besnard, C.; Kündig, E. P. *Chem. Sci.* **2013**, *4*, 1995. (b) Figg, T. M.; Wasa, M.; Yu, J. Q.; Musaev, D. G. *J. Am. Chem. Soc.* **2013**, *135*, 14206.
(30) Please see Figure S3 for more details about transformation of **P-Int6** to **P-Int7b**.
(31) (a) Ackermann, L. *Chem. Rev.* **2011**, *111*, 1315. (b) Lapointe, D.; Fagnou, K. *Chem. Lett.* **2010**, *39*, 1118.
(32) (a) Van Leeuwen, P. W. N. M.; Kamer, P. C. J.; Reek, J. N. H.; Dierkes, P. *Chem. Rev.* **2000**, *100*, 2741. (b) Marcone, J. E.; Moloy, K. G. *J. Am. Chem. Soc.* **1998**, *120*, 8527.
(33) In this context, we also considered the possibility that partial dissociation of dcype from Ni(II) center occurs before reductive elimination process. The free energy of the related three-coordinated transition state **P-TS4a** is +44.1 kcal/mol and thus was excluded. The details are given in Figure S5.
(34) Another reductive elimination pathway was also considered: **P-Int16** first dissociates CO to generate **P-Int10**, then transition state **P-TS4** occurs to give **P-Int11** (as shown in Figure 4). However, this CO dissociation-reductive elimination pathway needs to overcome an energy barrier of +32.9 kcal/mol, which is 4.0 kcal/mol higher than that of the direct-reductive elimination pathway ($\Delta G^{\ddagger}$ = +28.9 kcal/mol).
(35) (a) Hull, K. L.; Sanford, M. S. *J. Am. Chem. Soc.* **2009**, *131*, 9651. (b) Wei, Y.; Zhao, H.; Kang, J.; Su, W.; Hong, M. *J. Am. Chem. Soc.* **2010**, *132*, 2522.
(36) Kozuch, S.; Shaik, S. *Acc. Chem. Res.* **2011**, *44*, 101.
(37) For the details about CO extrusion of (dcype)Ni(CO) in eq 2, please see SI for more details.
(38) Similar observations has been also represented: (a) Quasdorf, K. W.; Antoft-Finch, A.; Liu, P.; Silberstein, A. L.; Komaromi, A.; Blackburn, T.; Ramgren, S. D.; Houk, K. N.; Snieckus, V.; Garg, N. K. *J. Am. Chem. Soc.* **2011**, *133*, 6352. (b) Mesganaw, T.; Silberstein, A. L.; Ramgren, S. D.; Nathel, N. F. F.; Hong, X.; Liu, P.; Garg, N. K. *Chem. Sci.* **2011**, *2*, 1766. (c) Gary, J. B.; Sanford, M. S. *Organometallics* **2011**, *30*, 6143.
(39) The five-centered oxidative addition transition states **T-TS5a** ($\Delta G^{\ddagger}$ = +16.5 kcal/mol) in eq 2 is more feasible than the three-centered one **T-TS5** ($\Delta G^{\ddagger}$ = +28.6 kcal/mol).
(40) The direct decarboxylation process of **P-Int19**/**T-Int11** is unfavorable, because it needs to overcome an energy barrier of +43.1/+53.9 kcal/mol. Please see SI for more details.
(41) The energy barrier of thiophene-2-carboxylic (of **P-Int19**) assisted C−H activation is as high as +46.7 kcal/mol (**P-TS8**), please see SI for more details. Therefore, **P-TS8a** is more plausible for the C−H activation of azole, and this is in accordance with Itami's recently experimental result that the rate of C−H/C−O coupling reaction could be accelerated by base.
(42) Herein, it is noted that the relative free energy of **P-Int20a** is −19.6 kcal/mol in eq 1, while it is −23.9 kcal/mol in eq 2.

$$\textbf{P-Int1} + K_3PO_4 \rightarrow C_4SH_3COOK + \textbf{P-Int20a} \qquad \Delta G = -19.6 \text{ kcal/mol}$$

$$\textbf{T-Int1} + K_3PO_4 \rightarrow {}^{t}BuCO_2K + \textbf{P-Int20a} \qquad \Delta G = -23.9 \text{ kcal/mol}$$

The observation is attributed to the formation of different sylvines with **P-Int20a**. Therefore, the relative free energy of **P-Int20a** is differentiated by 4.3 kcal/mol in different reaction systems (eq 1 or 2). Similar conclusion is also applicable to all subsequent species in Figure 6.